Detections of Minute Defects and Accurate Measurements of Distance & Area of Objects in Neutron Beam Computed Tomography and X-ray Radiography Images by a CAD Based on the De-Convolution Technique

Kui M. CHUI [1], Shyr L. CHUI [2], Shu Y. ZHANG [3], Eberhard LEHMANN[4], Anders KAESTNER[4], Andrew WRIDE [1], David B. STANFIELD [1]

[1] Image Enhancement Technology Ltd, 8 Gilbey Close, Ickenham, Uxbridge, Middlesex, UK, UB10 8TD. Phone: +44 1895 635203; e-mails:ming-chui@iet.org.uk, andrew.wride@lineone.net, dbs@iet.org.uk

[2]University Hospital of Northern British Columbia, BC, Canada. e-mail: shyrchui@netscape.net

[3]Science and Technology Facilities Council, Rutherford Appleton Laboratory, Didcot, Oxfordshire, OX11 0QX, UK. e-mail:shu-yan.zhang@stfc.ac.uk

[4]Spallation Neutron Source Division, Paul Scherrer Institut, ASQ Division WB BA/112, 5232 Villigen PSA., Switzerland. E-mails: eberhard.lehmann@psi.ch, anders.kaestner@psi.ch

Abstract

Blurred image edges caused by the Penumbra Effect have existed since the discovery of X-rays. In Computed Tomography (X-ray or Neutron-Beam), the combined effect of the size(s) of the energy source and the detector(s) cause the Penumbra Spread. Recently, by using the processing power of modern CPUs, we have found a software solution to the problem - a post-processing De-Convolution Technique for the detection, definition, and enhancement of image edge profiles. Enhancement is carried out in a zoomed space within which, the higher the magnification factor, the clearer the enhanced image, as both the Penumbra and the Pixelization Effects are overcome simultaneously. The overall effect is to re-focus the image edge-profile, as if derived from an infinitely small energy source. This patented technique has all the advantages of sensitivity, sub-pixel accuracy, and efficiency (in terms of processing-time). By solving this previously 'unsolvable' problem, numerous important applications may now be realized.

Keywords: Neutron Beam Computed Tomography, X-ray Radiography, Image Enhancement, De-Convolution Technique, Accurate Measurements, NDT.

1. Introduction

1.1 Object or Purpose of Study

The Penumbra Effect describes blurring at the margins of an image profile due to the finite size of the energy source. A computer aided detection (CAD) algorithm based on the De-Convolution Technique can be used to pinpoint true edge positions to sub-pixel accuracy and remove the Penumbra Effect (and at the same time, the removal of the Pixelization Effect) via sub-pixel transfers without trade-off losses [1]. Derived from this, a definitive method of accurate measurement may have been found. 50 slices of NBCT images on six cooling holes of a used jet turbine blade were analyzed to study the merits of the algorithm on both the detection of minute defects such as fractures and distortion and the accurate measurement of the cross-sectional areas of the cooling holes. Five sets of X-ray Radiographic images were also studied for accurate measurement and the detection of minute fractures.

2. Specific Experimental Details

2.1 Materials, Methods, and Procedures

2.1.1. Composite phantom and New-York Catphan-500 were used to provide X-ray CT images to verify the accuracies of the De-Convolution Technique [1 & Section 2.2].

2.1.2. The Technique of Neutron-Beam Computed Tomography (NBCT)

The neutron-beam imaging experiment was performed at the cold neutron imaging beamline ICON of the SINQ spallation neutron source at the Paul Scherrer Institut (PSI) [2]. The neutrons at the beamline originate from the cold moderator of the SINQ (25K) and have an energy spectrum with peak at 25meV and an average energy of 8.5meV. Using the high-resolution imaging setup at experiment position 2 and a neutron aperture of 20mm the collimation ratio was L/D=340. This was sufficient to assume parallel beam geometry for the given sample size. The pixel size was 13.5 microns and the resolution 21 lp/mm. The CT projection data consisted of 625 projections (2048x2048 pixels) on a 360 degrees scan. The projection data was reconstructed using a filtered back-projection algorithm for parallel beam.

2.2 Results

2.2.1 Phantom Calibration by X-ray CT

Measurements: Distance – at high-contrast and 1% low-contrast edge, both accurate to 1/50th of a pixel. Area/Volume - at high-contrast and 1% low-contrast edge, accurate to 1/18th and 1/10th of a pixel respectively. Modulation Transfer Function (MTF) [3] – improved from 3.38 lp/cm to 9.61 lp/cm at 50% modulation level after 7x magnification and enhancement. Processing time - 7x magnification and enhancement of region of interest (ROI) of size 107x107 pixel^2 (or 749x749 sub-pixel^2) took 1.17 seconds using a 2.4GHz-CPU.

2.2.2. NBCT images – 505 Neutron-Beam CT image slices through a jet turbine blade, end to end, (0.013mm/slice) were collected.

2.2.2.1. Field Examples

A used Tornado jet engine turbine blade (C3FOX) was analyzed. To cover the complete blade, 505 slices of thickness 0.0135mm/slice were obtained. 50 slices starting from #0520, #0530, (step 10), ... to #1010 were analyzed. An additional noise filter was added in to help with the analysis. Figure 1 shows the original image of Slice #0520 with ROI placed on the six cooling holes of A, B, C, D, E & F. Figure 2 - the 7x magnification of ROI on the six holes 'after' enhancement.

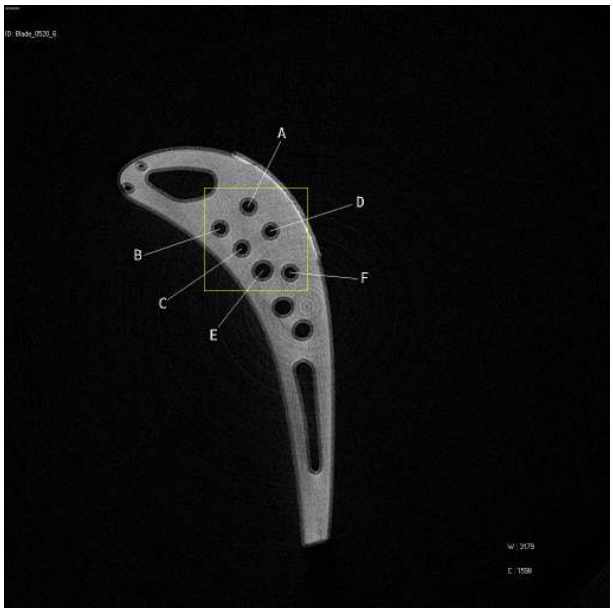

Figure 1–Original image of #0520 with ROI on 6 holes.

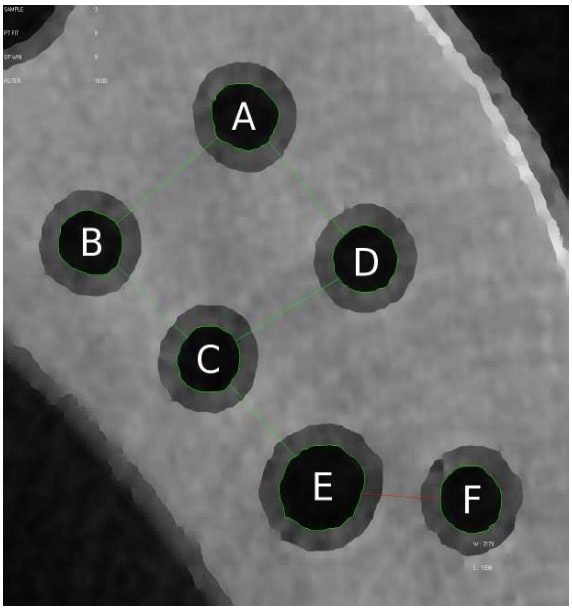

Figure 2–7xROI 'after' enhancement with annotations.

2.2.2.2. Image examples of step-by-step edge-profile detection and enhancement with ROI placed on Hole B of Slice # 0620:-

Figure 3 - Original image of #0620 with ROI on Hole B, Figure 4 - 7xROI on Hole B 'before' enhancement, Figure 5 – 7xROI on Hole B 'before' enhancement with edge-dot profiles detected, Figure 6 – 7xROI on Hole B 'after' enhancement with edge-dot profiles, Figures 7 & 8 are images of 'before' (left) and 'after' (right) enhancement without edge-dot profiles placed side-by-side for their comparison, and Figure 9 - 7xROI on Hole B 'after' enhancement with edge-dot profiles and outlining drawn for area measurement.

Figure 3 - Original image of #0620 with ROI on Hole B.

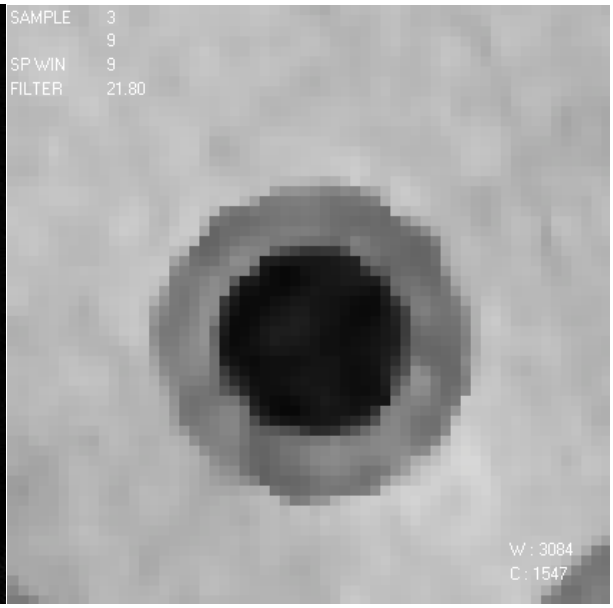

Figure 4 - 7xROI on Hole B 'before' enhancement.

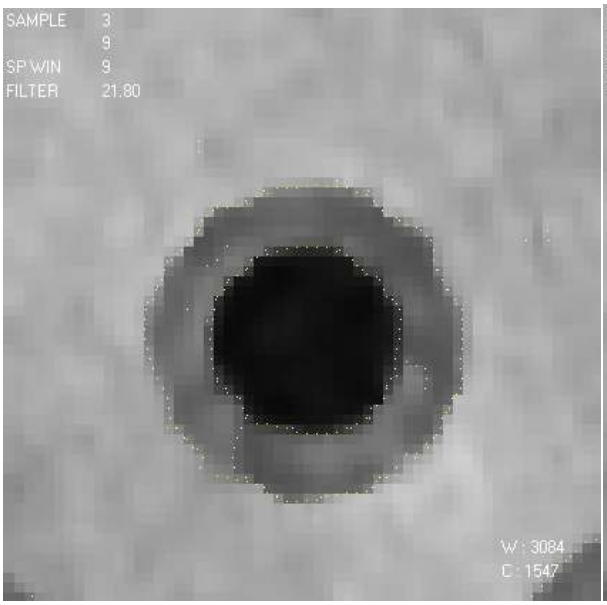

Figure 5 – 7xROI on Hole B 'before' enhancement with edge-dot profiles detected.

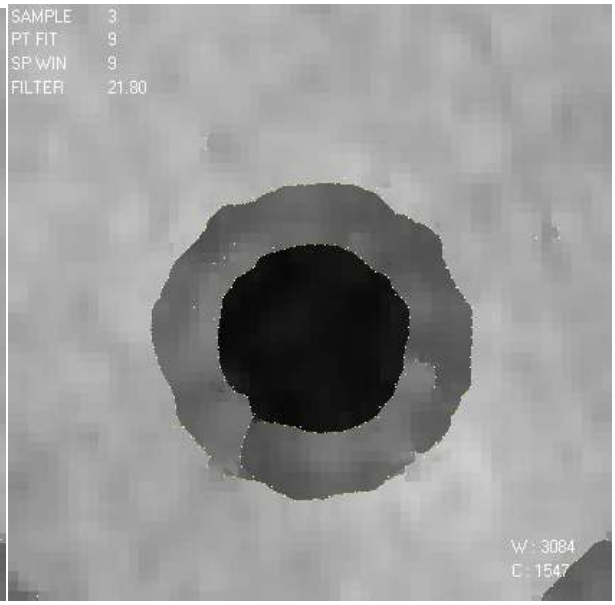

Figure 6 – 7xROI on Hole B 'after' enhancement with edge-dot profiles,

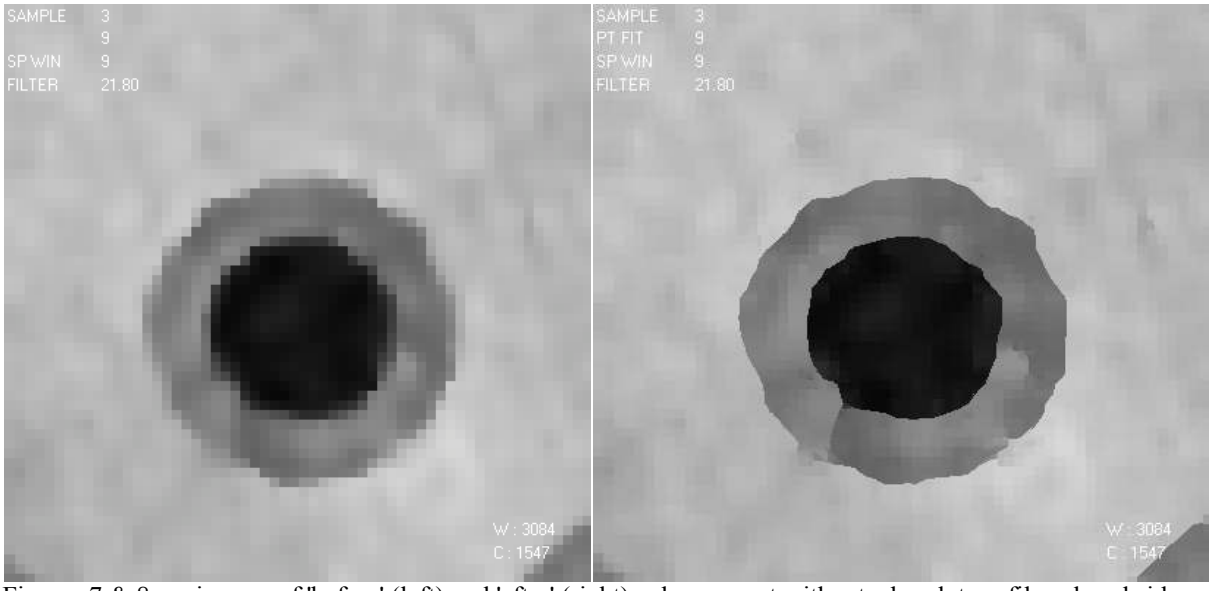

Figures 7 & 8 are images of 'before' (left) and 'after' (right) enhancement without edge-dot profiles placed side-by-side for their comparison.

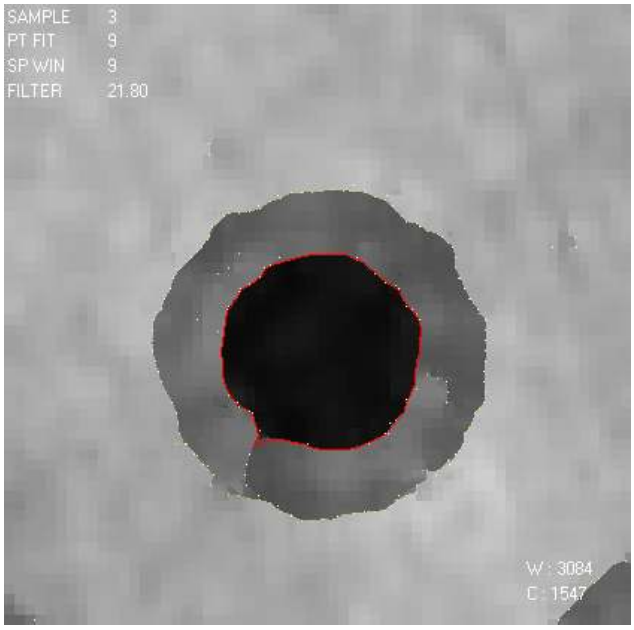

Figure 9 - 7xROI on Hole B 'after' enhancement with edge-dot profiles and outlining drawn for the following area measurement:

Measurement: Area = 285 pixel^2 => 0.0495 mm^2.

2.2.2.3. Cross-Sectional Area

The cross-sectional area of the six cooling holes, A, B, C, D, E, & F versus the 50 slice positions were measured and plotted in Figure 10.

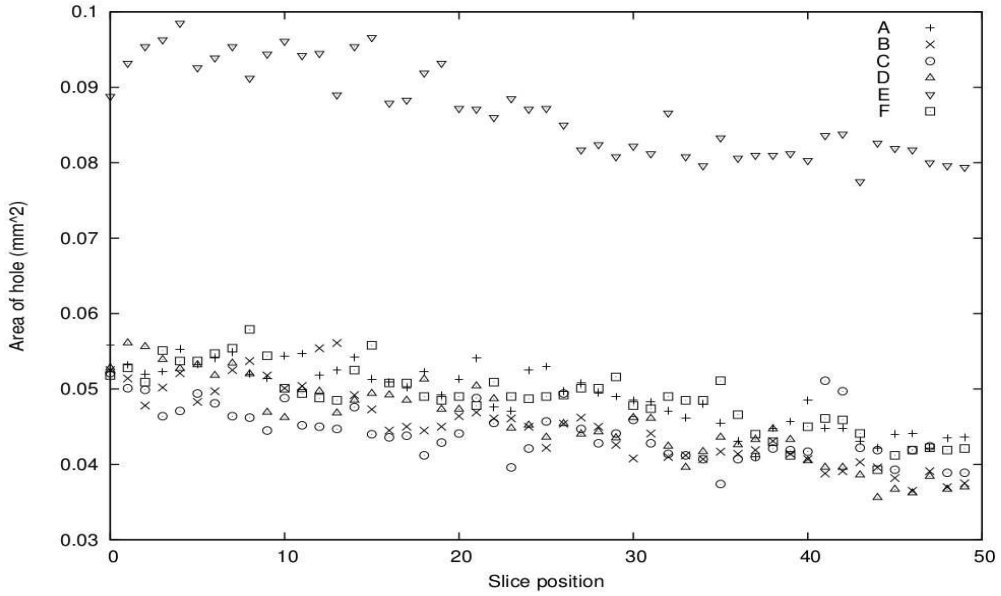

Figure 10: Area of cooling hole versus slice-position

The areas of the six holes varied across the slice set (Table 1).

Table 1. Areas of Holes

Hole	Max. (mm^2)	Min. (mm^2)	Diff. (%)
A	0.0558	0.0410	36.10
B	0.0561	0.0365	53.70
C	0.0521	0.0374	39.30
D	0.0561	0.0356	57.58
E	0.0985	0.0775	27.10
F	0.0579	0.0393	47.33

2.2.2.4. Inter-Hole Distances

Inter-hole distances were also measured, and means and standard deviations calculated (Table 2).

Table 2. Inter-Hole Distances

Holes	Mean Distance (mm)	Standard Deviation
AB	0.515	1.78E-02
BC	0.411	9.34E-03
CD	0.486	1.56E-02
DA	0.496	1.30E-02
CE	0.381	1.60E-02
EF	0.319	8.95E-03

2.2.2.5. Distortion

For example, Hole A in Slice #0630 (Figure 11) exhibited a non-circular distorted shape of:

Diameter (major length at 151.9 degree) = 0.28 mm.

Diameter (minor length at 64.0 degree) = 0.24 mm.

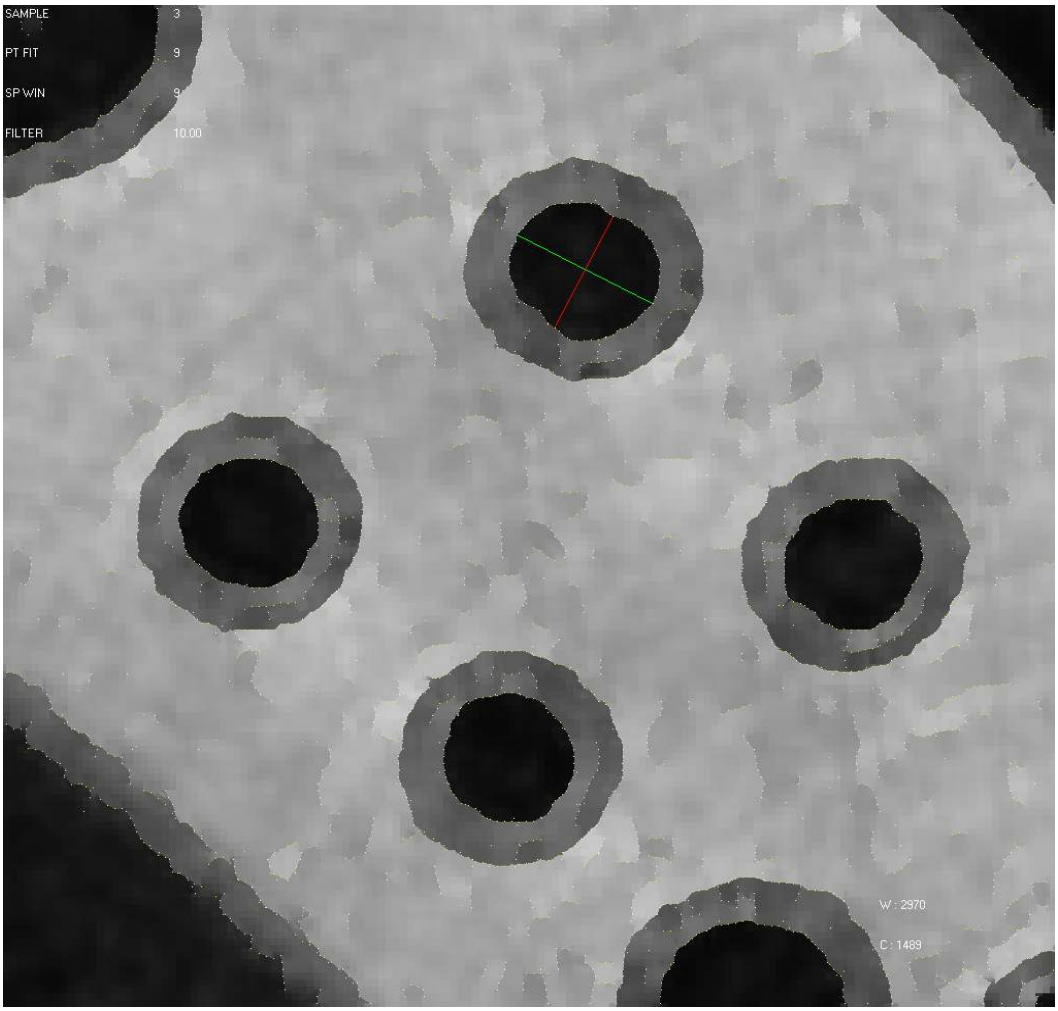

Figure 11: Distortion at Hole A of Slice #0630

2.2.2.6. Fractures

2.2.2.6.1. Small fractures were observed at Hole D in Slice #0850 (Figure 12) and at Hole B in Slice #0885 (Figure 13).

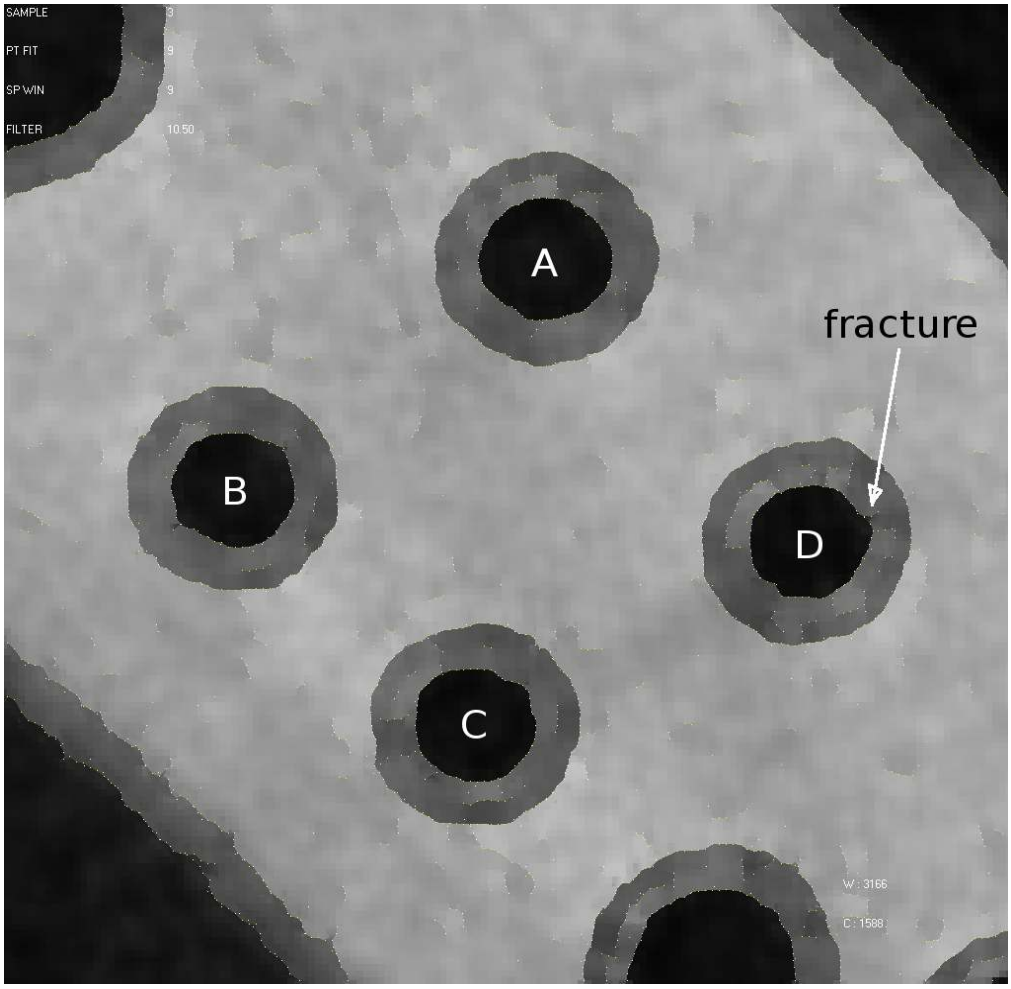

Figure 12: Fracture at Hole D of Slice #0850

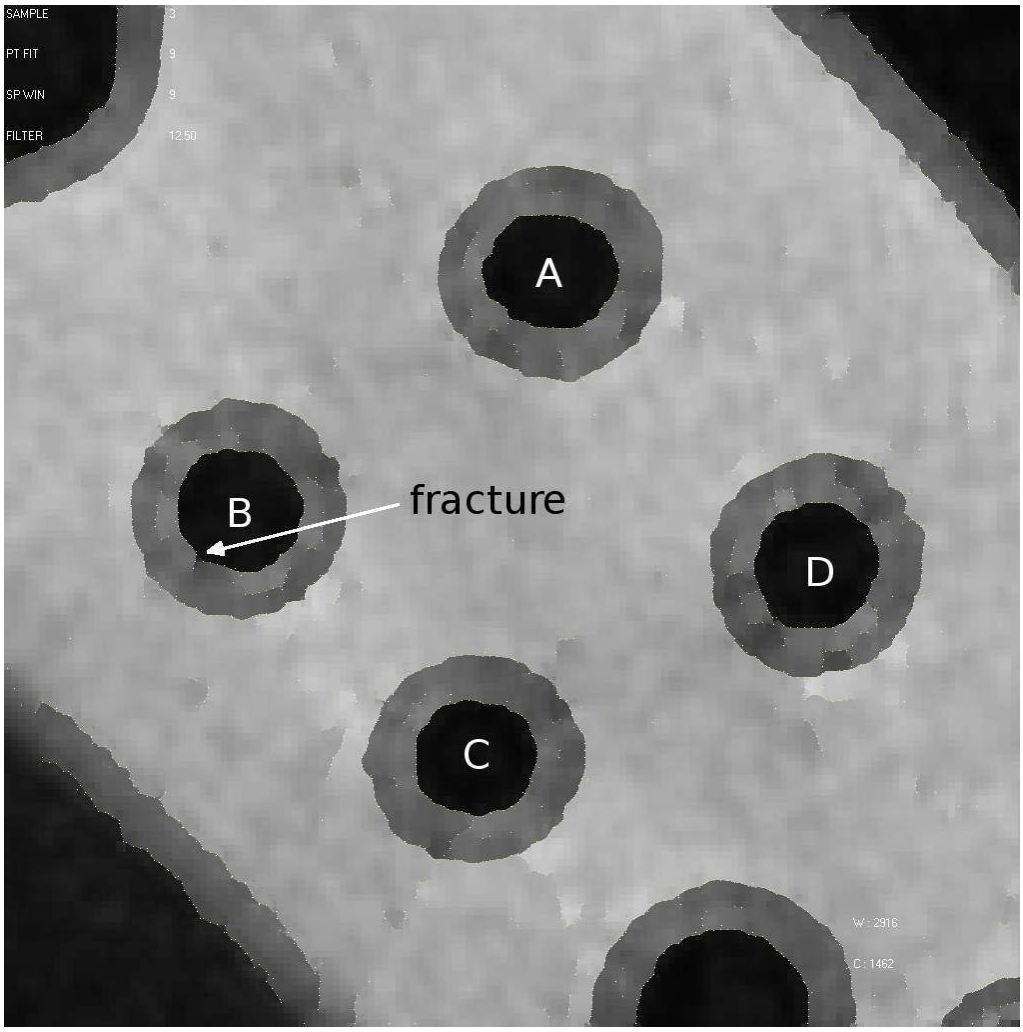

Figure 13: Fracture at Hole B of Slice #0885

2.2.2.6.2. A longer fracture was observed at Hole B in Slice #0620 (Figure 14)

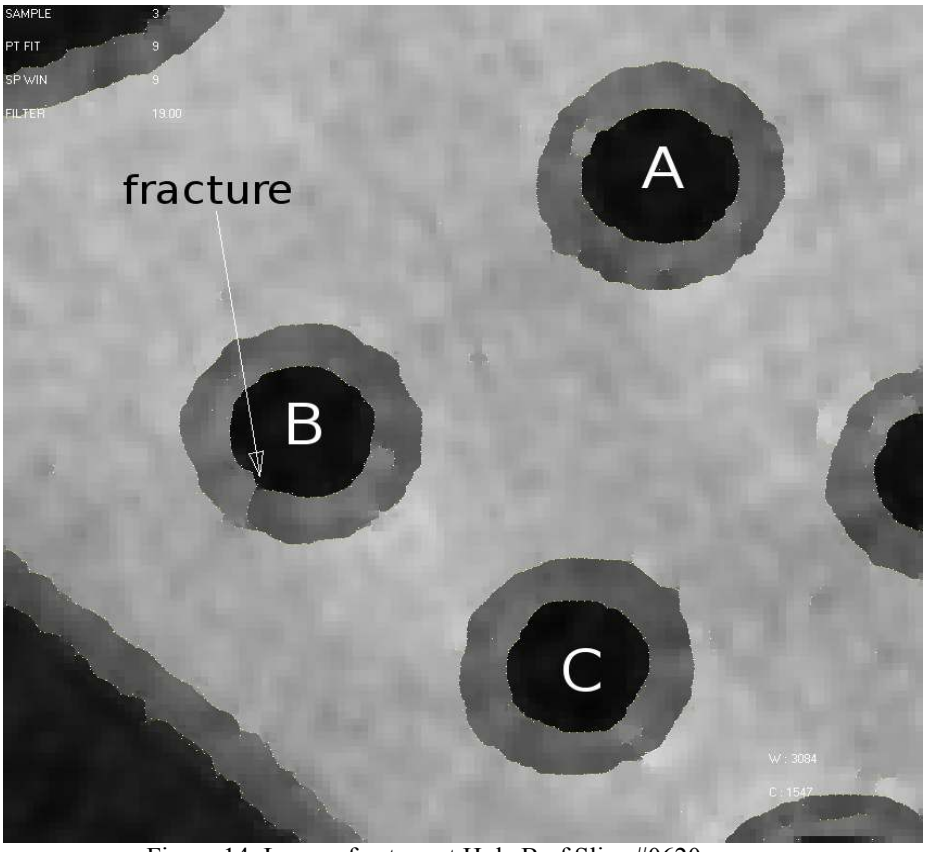

Figure 14: Longer fracture at Hole B of Slice #0620

2.2.3. X-ray Radiographic Images:

2.2.3.1. - X-ray Radiogram of a Guide Wire within a Phantom. A Guide Wire was used to study the enhancement by the CAD:- Figures 15 & 16 showed the 'before' and 'after' enhancement of 7xROI on a Guide Wire.

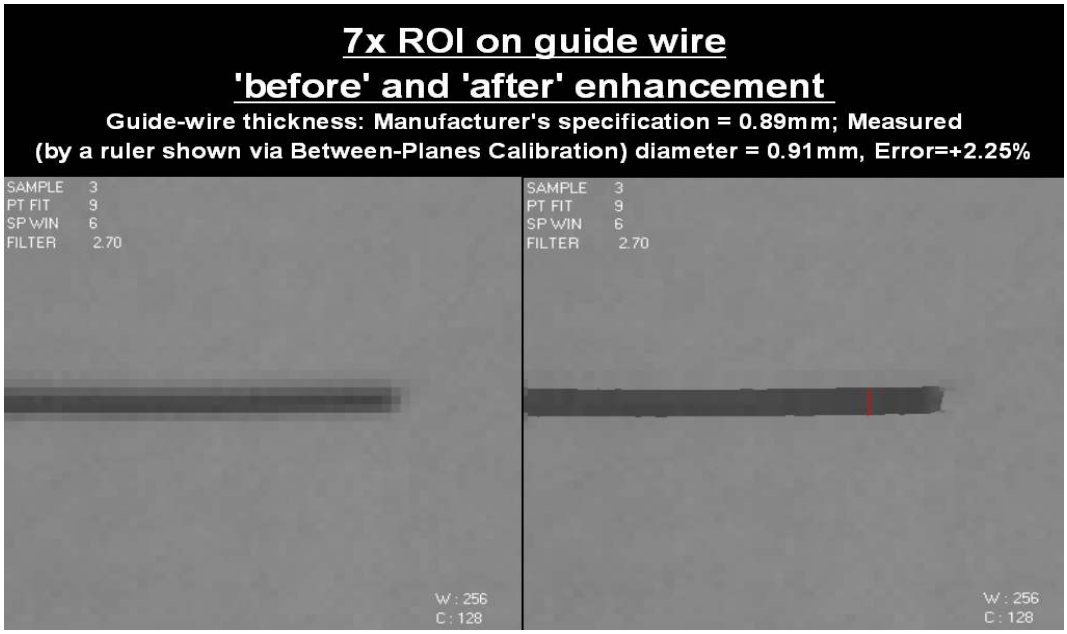

Figures 15 & 16 are the 'before' (left) and 'after' (right) placed side-by-side for comparison.

Measurement of thickness:- By a Software Ruler of CAD = 0.91mm against Manufacturing Specification of 0.89mm. => Experimental Error = +2.25%.

2.2.3.2. - X-ray Image of a 'Star' Shape Fracture within a Machined Component:

The following Figures 17 & 18 showed the 'before' and 'after' enhancement of 7xROI on a 'Star ' shape fracture of a machined component.

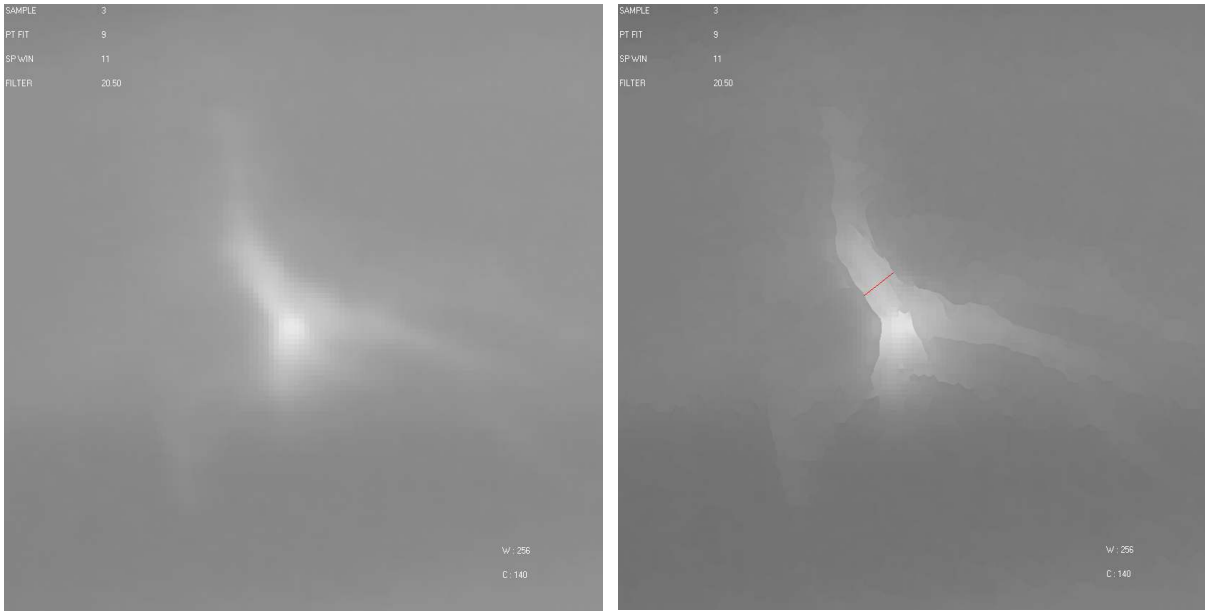

Figures 17 & 18 are the 'before' (left) and 'after' (right) enhancement of 7x ROI on a 'Star' shape fracture in a machined component.

Indicated width measured = 7.54 pixels. Absolute measurement would be possible if calibrated with a known width such as the diameter of a ball bearing placed near the effect.

2.2.3.3. - Due to the lack of page space, three more sets of X-ray radiographic images of low-contrast fractures will be presented in the PowerPoint slide-set once accepted.

4. Conclusions

Detection of minute defects and hyper-accurate area and width measurements of small structures are now possible. The technique may be used for:

(a) Quality control during the original manufacturing process of components.

(b) The monitoring of the condition of in-service components prior to reuse.

5. References

1."A De-Convolution Technique used for NDT in X-ray & CT", by Kui M. Chui, Shyr L. Chui, Andrew Wride, & David B. Stanfield, Oral/Full paper presentation in 17th World Conference on Non-destructive Testing (17WCNDT), Shanghai, China, October 25-28, 2008. (www.NDT.net - The e-Journal & Database of Non-Destructive Testing - ISSN 1435-4934).

2."The ICON beamline - A facility for cold neutron imaging at SINQ", by A. Kaestner, S. Hartmann, G. Kuehne, G. Frei, C. Gruenzweig, L. Josic, F. Schmid, E. Lehmann, Nuclear Instruments and Methods in Physics Research Section A: Accelerators, Spectrometers, Detectors and Associated Equipment 659(1), 2011, pp. 387-393.

3."The line spread function and modulation transfer function of a computed tomographic scanner". Judy P.F., Med. Phys. Vol.3, No. 4, Jul/Aug. 1976, pp.233-236.